Use of a Flowing Afterglow SIFT Apparatus To Study the Reactions of Ions with Organic Radicals†

Xu Zhang, Shuji Kato, Veronica M. Bierbaum, Mark R. Nimlos,‡ and G. Barney Ellison*

Department of Chemistry & Biochemistry, University of Colorado, Boulder, Colorado 80309-0215

Received: May 21, 2004; In Final Form: August 5, 2004

This paper describes a new technique for the experimental study of ions with organic radicals. A preliminary report has been published in *J. Chem. Phys.* **2004**, *120*, 3531, and we wish to communicate a complete description of this experiment. Clean, intense flows of hydrocarbon radicals/diradicals can be produced by a heated supersonic nozzle and are delivered to a flowing afterglow selected ion flow tube (FA-SIFT) instrument. The reactions of a simple radical, allyl (CH_2CHCH_2), and a diradical, *ortho*-benzyne (*o*-C_6H_4), with hydronium (H_3O^+) and hydroxide (HO^-) ions were studied at thermal energy. We have studied the following reactions: $CH_2CHCH_2 + H_3O^+ \rightarrow C_3H_6^+ + H_2O$, $CH_2CHCH_2 + HO^- \rightarrow$ no product ions, *o*-$C_6H_4 + H_3O^+ \rightarrow C_6H_5^+ + H_2O$, and *o*-$C_6H_4 + HO^- \rightarrow C_6H_3^- + H_2O$. We find that proton transfer reactions with H_3O^+ occur rapidly (the bimolecular rate constant, k^{II}, is roughly 10^{-9} cm^3 s^{-1}). However, an unexpected result was obtained for *o*-$C_6H_4 + HO^-$; the exothermic proton abstraction is significantly slower than the collision rate by nearly an order of magnitude (k^{II} is approximately 10^{-10} cm^3 s^{-1}). We rationalize this by postulating a competing associative detachment. No charged products have been observed for $CH_2CHCH_2 + HO^-$, presumably because of similar detachment pathways.

Introduction

Ions and radicals are both reactive species. Recently,[1] we published a short note that describes results from a new approach to study reactive collisions between simple ions and organic radicals. In this paper, we provide a much more thorough description of this new experiment.

Over recent decades, molecular beam and flow tube techniques have been used to explore the spectroscopy and chemistry of ions and radicals. Thousands of ion reactions have been studied with stable neutrals and with some atomic radicals in the gas phase,[2] with the aim of understanding the fundamental chemical reaction dynamics as well as the chemistry of the earth's upper atmosphere, interstellar medium, and plasma phenomena such as lasers.[3−6] Chemical ionization mass spectrometry has begun to use some ion/radical reactions to monitor the atmospheric chemistry of radicals.[7−9]

In contrast, reactions of gas phase ions with polyatomic hydrocarbon radicals have rarely been studied because of the inherent experimental difficulties. It has been known[10,11] that ion−molecule reactions involving open shell, radical ions ($A^{\bullet -} + BC \rightarrow$ products) are generally more complex and unpredictable than are those with closed-shell ions ($A^- + BC \rightarrow$ products). In reactions of an ion with an organic radical ($A^- + BC^{\bullet} \rightarrow$ products), the charge and radical sites are split between the collision partners (and the ion can be an open shell ion). The fundamental chemistry in these systems remains largely unexplored.

Ion−organic radical reactions are also expected to be important in several environments, including in combustion processes. Here, the elevated temperatures generate high densities of energetic species that react rapidly to synthesize a myriad of combustion products. In oxyacetylene flames,[12] HCO^+, $C_3H_3^+$, H_3O^+, HC_2^-, O_2^-, CN^-, and HO^- have been identified as major ions at densities of 10^8-10^{10} cm^{-3}. A proton transfer reaction between HCO^+ and C_3H_2 carbene has been proposed as a possible source for $C_3H_3^+$, while a charge transfer equilibrium between HC_2^- and a CN radical may be a source[12] of observed CN^-. Within the interstellar medium, large polycyclic aromatic hydrocarbons (PAHs) have been suggested as carriers of the unidentified infrared emissions and of the diffuse interstellar bands.[13−15] Radioastronomy has detected more than a hundred organic species in the interstellar medium,[16] among them about one-third are radicals or carbenes and several are ions. The mechanisms of formation of these polyatomic species remain unknown, but reactions of ions with radicals are believed to be a central component in their formation. Ion−radical reactions may also be important in the upper regions of the earth's and other planets' atmospheres.

Experimental investigations of ion−organic radical reactions are challenging primarily because of the difficulty in generating the radicals cleanly and at high densities. Reactant ions and radicals may be lost easily, before their mutual encounter, by reactions with their chemical precursors, by collisions with the wall, and by radical−radical reactions. In a flowing afterglow selected ion flow tube (FA-SIFT) instrument, the reaction time is roughly 10 ms. To generate detectable amounts of product ions, the density of the radicals in the FA-SIFT reaction flow tube must be at least 10^9 radicals cm^{-3}. In comparison, atomic radicals can be generated relatively easily by dissociation of their precursors in a microwave discharge or over a heated metal surface. These radical sources have been combined with the FA-SIFT or Fourier transform ion cyclotron resonance (FT-ICR) instruments to study reactions of H, N, and O atoms.[17−19]

† Part of the special issue "Tomas Baer Festschrift".

* E-mail: barney@jila.colorado.edu.

‡ National Renewable Energy Laboratory, 1617 Cole Blvd., Golden, CO 80401.

10.1021/jp047792u CCC: $27.50
Published on Web 10/01/2004

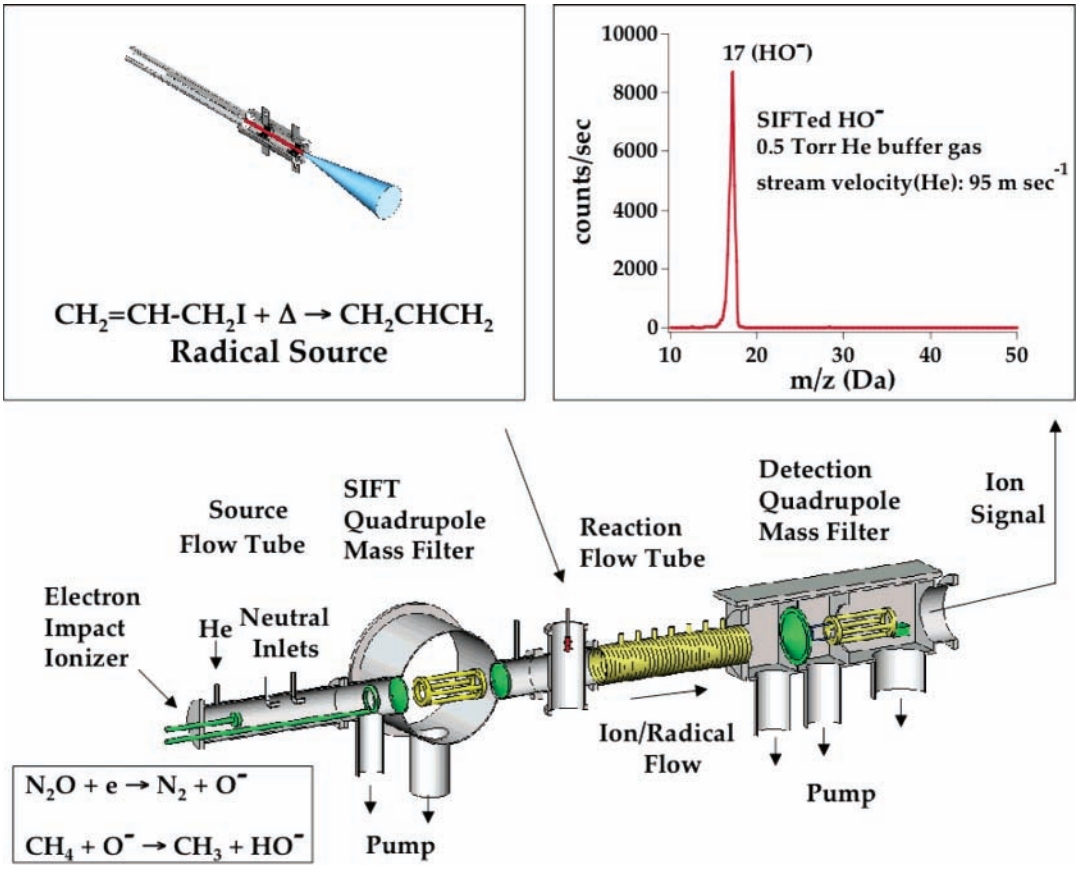

Figure 1. SIFT instrument with a hyperthermal radical source.

We have employed a new approach that combines a heated supersonic nozzle[20] with the FA-SIFT instrument[21] (Figure 1). Thermal decomposition of a variety of organic compounds in a pulsed supersonic nozzle produces clean, intense beams of organic radicals or diradicals;[22] typical nozzle temperatures range from 300 to 1800 K with a short pyrolysis time of about 30 μs. The SIFT instrument was developed to generate mass-selected ions in a helium buffer gas (65 Pa or 0.5 Torr) free from their chemical precursors. The high pressure flow tube environment allows both the ions and radicals to be thermally equilibrated (roughly 300 K) before they react; the occurrence of 10^4 to 10^5 collisions with the He buffer gas facilitates complete relaxation of vibration except for small nonpolar diatomics.[23] The flow tube also provides a moderately long reaction time of roughly 10 ms.

In a recent note, we reported[1] the first observation of ion reactions with hydrocarbon radicals and diradicals using the flowing afterglow technique. A simple radical, allyl (CH_2CHCH_2), and a diradical, *ortho*-benzyne (*o*-C_6H_4), were produced in a hyperthermal nozzle [eqs 1 and 2, where Δ represents heat].

$$CH_2{=}CH{-}CH_2I + \Delta \rightarrow CH_2CHCH_2 + I \qquad (1)$$

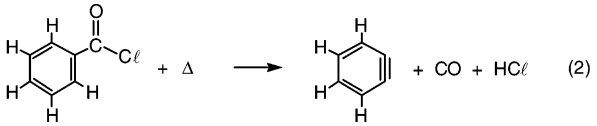

(2)

We demonstrated that these radicals react with the simple gas phase ions, hydronium cation (H_3O^+) and hydroxide anion (HO^-).

$$CH_2CHCH_2 + H_3O^+ \rightarrow C_3H_6^+ + H_2O \qquad (3)$$

$$CH_2CHCH_2 + HO^- \rightarrow \text{no product ions} \qquad (4)$$

$$o\text{-}C_6H_4 + H_3O^+ \rightarrow C_6H_5^+ + H_2O \qquad (5)$$

$$o\text{-}C_6H_4 + HO^- \rightarrow C_6H_3^- + H_2O \qquad (6)$$

Experimental Methods

Figure 1 provides an overview of the FA-SIFT instrument[21] coupled with a hyperthermal nozzle.[20,22] H_3O^+ or HO^- ions are generated in the source flow tube by electron impact and ion−molecule reactions (eqs 7−11). H_3O^+ ions are produced by electron impact on He, generating He^+ and metastable He*, followed by charge transfer or Penning ionization of H_2O with He^+ and He*; the resulting H_2O^+ reacts with H_2O to afford hydronium ions. HO^- ions are generated by electron impact on N_2O to form O^-, which further reacts with CH_4 via hydrogen atom transfer to form hydroxide ions.

$$\mathbf{H_3O^+}\text{: } He + e \rightarrow He^+, He^* \qquad (7)$$

$$(He^+, He^*) + H_2O \rightarrow H_2O^+ \qquad (8)$$

$$H_2O^+ + H_2O \rightarrow H_3O^+ + HO \qquad (9)$$

$$\mathbf{HO^-}\text{: } N_2O + e \rightarrow N_2 + O^- \qquad (10)$$

$$CH_4 + O^- \rightarrow CH_3 + HO^- \qquad (11)$$

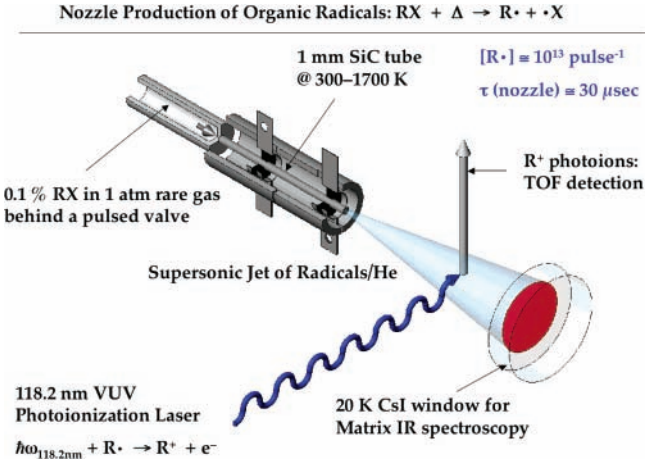

Figure 2. Diagram of the hyperthermal nozzle, matrix deposition IR system, and photoionization source.

The ions are then "SIFTed", that is, mass selected with the SIFT quadrupole mass filter and injected into the reaction flow tube (7.3 cm inner diameter and roughly 1 m long) containing a helium buffer gas (0.5 Torr, ≅300 K) flowing at a velocity of about 95 m s^{-1}. The SIFT injection produces a continuous flow of ions (approximately 10^5 particles cm^{-3}) in a stream of helium. The ions are isolated from their chemical precursors, and the flow tube environment allows them to be thermally equilibrated (≅300 K) before ion−radical reactions take place.[21] Since the reaction flow tube in Figure 1 is 1 m long from the radical source to the detection quadrupole mass filter, the gas transit time is approximately 10 ms down the flow tube. The ionic species (both the reactant and products) are detected using the quadrupole mass spectrometer at the end of the flow tube. The inset in Figure 1 shows pure HO^- ions with no radicals introduced, and with a very low background signal (less than 1 count s^{-1}).

Figure 1 shows a radical source mounted on the flow tube after the SIFT quadrupole mass filter. Streams of CH_2CHCH_2 radicals or *o*-C_6H_4 diradicals are generated through pyrolysis of allyl iodide (CH_2CHCH_2I) and benzoyl chloride (C_6H_5COCl), respectively. Allyl iodide or benzoyl chloride seeded in helium (roughly 65 Pa in 8×10^4 to 1×10^5 Pa or 0.5 Torr in 600−800 Torr) passes through a pulsed valve (20−40 Hz) into the resistively heated SiC nozzle (approximately 1×10^3 Pa or 10 Torr). The pyrolysis products along with the He carrier gas expand supersonically through the nozzle into the flow tube for a duration of 1.3 ms.

To ensure that our heated supersonic jet is producing the desired target radicals, we have mounted the radical source on an instrument that can use infrared absorption spectroscopy or photoionization mass spectroscopy (PIMS) to characterize the resultant molecular beam. Figure 2 illustrates an overview of the hyperthermal nozzle, photoionization source, and matrix deposition system. Photoionization time-of-flight mass spectrometry and matrix isolation infrared spectrometry measurements were employed to monitor the pyrolytic generation of the allyl radical and *o*-benzyne. A detailed description of these two techniques has been described elsewhere.[22]

The nozzle temperature has been measured with a thermocouple attached to the external surface. In the PIMS and matrix isolation measurements, the actual pyrolysis temperature inside the nozzle is approximately 200 K higher because of the radiative heat loss from the SiC surface.[22] When deployed on the SIFT experiment (Figure 1), the nozzle surface will be cooled by conductive heat transfer to the helium buffer gas (0.5 Torr). Therefore, the measured external nozzle temperature in the SIFT experiment is about 200 K lower than those in the PIMS and matrix experiments.

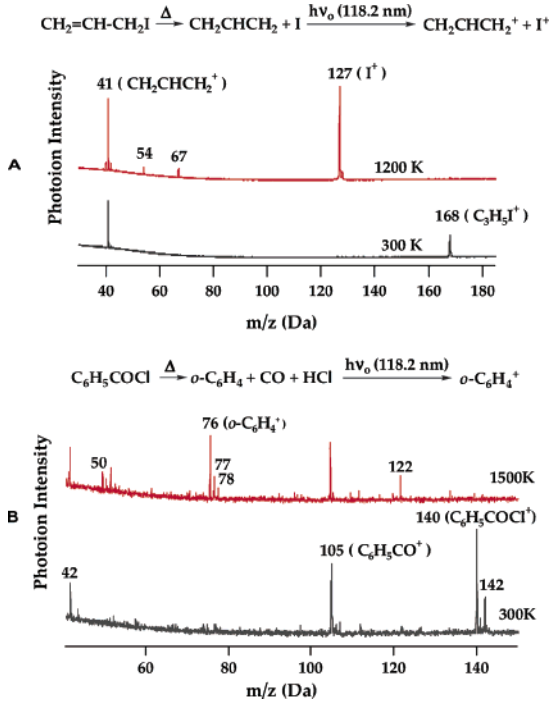

Figure 3. Photoionization TOF mass spectra from hyperthermal nozzle decomposition of (A) allyl iodide and (B) benzoyl chloride. Reference spectra with the nozzle unheated (300 K) are also shown in the bottom traces.

In the PIMS experiment in Figure 2, the ninth harmonic (118.2 nm or 10.487 eV) of the Nd:YAG laser output has been used to ionize the radicals emitted from the nozzle; ionization energies for the allyl radical[24,25] and *o*-benzyne[26] are 8.153 ± 0.001 eV and 9.03 ± 0.05 eV, respectively. Figure 3 shows the PIMS spectra that demonstrate the allyl radical production at *m*/*z* 41 ($CH_2CHCH_2^+$) and *o*-benzyne production at *m*/*z* 76 (*o*-$C_6H_4^+$) at the nozzle temperatures of 1200 and 1500 K, respectively. The allyl radical and *o*-benzyne are detected at *m*/*z* 41 ($CH_2CHCH_2^+$) and *m*/*z* 76 (*o*-$C_6H_4^+$), respectively. In Figure 3A, the bottom trace (black) shows ions resulting from ionization of allyl iodide via a room temperature nozzle. Peaks at *m*/*z* 168 ($C_3H_5I^+$) and *m*/*z* 41 ($C_3H_5^+$) arise from ionization and ionization dissociation, respectively, of the precursor. The top trace (red) shows the signal when allyl iodide is injected via the hyperthermal nozzle at a nominal temperature of 1200 K. The precursor is completely decomposed and the $C_3H_5I^+$ peak disappears, while peaks due to allyl radicals and iodine atoms, $CH_2CHCH_2^+$ (*m*/*z* 41) and I^+ (*m*/*z* 127), are present. The two small peaks at *m*/*z* 54 and 67 arise from ionization dissociation of 1,5-hexadiene, the recombination product of two allyl radicals. In Figure 3B, the bottom trace (black) shows ions resulting from ionization of benzoyl chloride via a room temperature nozzle. Peaks at *m*/*z* 140 and 142 belong to the precursor, $C_6H_5COCl^+$, at natural chlorine abundance. The ion $C_6H_5CO^+$ at *m*/*z* 105 arises from ionization dissociation of C_6H_5-COCl. The feature at *m*/*z* 42 belongs to an added mass marker, propene ($C_3H_6^+$). At a nominal temperature of 1500 K (top trace in red), the precursor has largely decomposed to form *o*-benzyne, shown at *m*/*z* 76 (*o*-$C_6H_4^+$). The persistent signal at *m*/*z* 105 is attributed to ionization dissociation of the residual precursor and not photoionization of C_6H_5CO radicals; there is evidence for thermally enhanced ionization dissociation of the precursor.

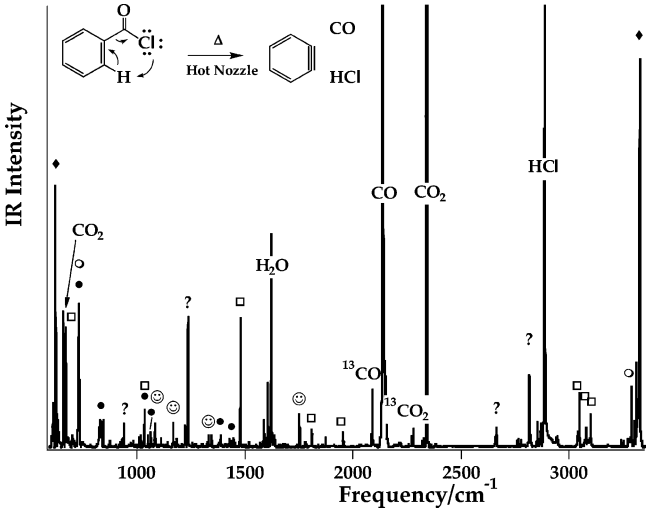

Figure 4. Matrix IR spectrum from thermal decomposition of benzoyl chloride at a nominal temperature of 1600 K. *o*-benzyne along with HCl and CO, the thermal decomposition products of benzoyl chloride, are observed. Also present in the spectrum are diacetylene (HC≡C−C≡CH) and acetylene (HC≡CH), which are derived from *o*-C_6H_4. A small amount of benzoic acid (C_6H_5COOH) generated from hydrolysis of benzoyl chloride (C_6H_5COCl) is detected in the spectrum. Benzene that may arise from secondary reactions of *o*-benzyne and/or thermal decomposition of benzoic acid is also observed. The peak assignments[28−32] (in cm^{-1}) follow. The unknown bands (indicated with ?) may come from impurities in the sample line or from the hot nozzle itself. *o*-C_6H_4 (●): 737, 849, 1041, 1054, 1392, 1448; C_4H_2 (◆): 628, 3326; C_2H_2 (○): 737, 3298; C_6H_6 (□): 675, 1041, 1483, 1812, 1956, 3047, 3079, 3100; C_6H_5COOH (smiling face): 1067, 1088, 1171, 1349, 1753. Unknown species (?): 943, 1240, 2664, 2815.

Thermal cracking of *o*-benzyne produces diacetylene and acetylene; *o*-$C_6H_4 + \Delta \rightarrow$ HC≡C−C≡CH + HC≡CH. Beside the spurious noise signals, the peak at *m*/*z* 50 corresponds to ionized diacetylene $(HC{\equiv}C{-}C{\equiv}CH)^+$, while ionization of acetylene (HC≡CH) is not possible due to its high ionization energy[27] (*IE* = 11.4 eV). The peak at *m*/*z* 122 is benzoic acid $(C_6H_5COOH)^+$, which is an impurity of the precursor generated by the hydrolysis of benzoyl chloride. Small peaks at *m*/*z* 77 and 78 are attributed to phenyl radical ($C_6H_5^+$) and benzene ($C_6H_6^+$), respectively, which may come from secondary reactions of *o*-benzyne and/or thermal decomposition of benzoic acid.

Our testing apparatus for the hyperthermal nozzle in Figure 2 is configured with a cold CsI window for vibrational spectroscopy. In the matrix isolation IR spectrometry measurement, the spectra are recorded with an MCT-A detector (4000−600 cm^{-1}, $D^* = 5 \times 10^{10}$ cm $Hz^{1/2}$ W^{-1}) in the IR spectrometer (Nicolet Magna 550). Figure 4 is the IR spectrum of benzoyl chloride (C_6H_5COCl) pyrolysis at 1600 K, which shows[28] the generation of *o*-C_6H_4. Diacetylene (HC≡C−C≡CH) and acetylene (HC≡CH), which arise from further thermal cracking of *o*-C_6H_4, are also observed[29] in the spectrum. Benzoic acid (C_6H_5-COOH), an impurity of benzoyl chloride (C_6H_5COCl) generated through hydrolysis, can be observed[30] in the spectrum. Benzene (C_6H_6), which may be produced from secondary reaction of *o*-benzyne and/or from pyrolysis of benzoic acid (C_6H_5COOH), is also detected.[31,32] From the IR intensities of *o*-benzyne, acetylene, and benzene, we estimate the conversion efficiency of C_6H_5COCl to *o*-C_6H_4 is roughly 60 ± 10%. The IR spectrum of the allyl radical (CH_2CHCH_2) generated from pyrolysis of allyl iodide has been detected earlier.[22,33] The conversion efficiency of allyl iodide to allyl radical is estimated to be 90% ± 10%.

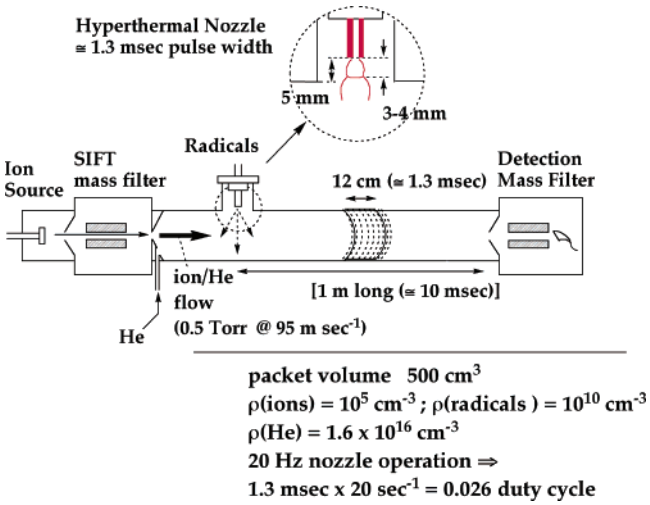

Figure 5. Schematic of the radical pulse mixing with the ion/He flow to generate an ion/radical packet (or reaction zone).

In the SIFT experiment, the hyperthermal radical source (SiC, 1 mm inner diameter and 2.5 cm long) is attached perpendicularly to the SIFT flow tube near its upstream end (Figure 1 and its inset). The nozzle tip is positioned 5 mm behind the inner surface of the flow tube so that it does not disturb the buffer gas flow while ensuring an efficient delivery and mixing of the pulsed jet of radicals into the stream of helium.[34,35] Figure 5 schematically shows the flow and reaction characteristics of ions and radicals in the SIFT experiments when the radical pulse is merged and mixed with the ion/He flow. Under the SIFT experimental conditions, we estimate that approximately 3×10^{13} CH_2CHCH_2 radicals or *o*-C_6H_4 diradicals are produced per pulse based on the precursor conversion efficiencies of 90% and 60%, respectively.[22] These radicals, plus helium atoms, are ejected from the nozzle for a total of $(5-8) \times 10^{16}$ particles per pulse with a duration of roughly 1.3 ms.

Given the mass flow and duration of the pulsed gas, along with the residence time (roughly 30 μs) in the nozzle,[22] the gas pressure is estimated to be about 1×10^3 Pa (or 10 Torr) inside the heated SiC tube. Since the pressure difference between the nozzle and flow tube (0.5 Torr) is low, the supersonic expansion from the nozzle is fairly weak; the location of the Mach disc is estimated to be 3−4 mm from the nozzle exit with a calculated terminal Mach number of 6−7 (Figure 5).[36] The Prandtl relationship for shock recovery[37] predicts the pressure to range from about 1.3 to 80 Pa (or 1×10^{-2} to 0.6 Torr) across the Mach disc. The post-recovery pressure is only slightly higher than the background pressure of helium, so that reexpansion of the flow is also expected to be weak. Overall, the directional flow of radicals is expected to persist no farther than 10 mm from the nozzle exit. The weak expansion combined with the close proximity of the nozzle to the main He stream ensures that the radical pulse is rapidly mixed with the flow tube helium and thermally equilibrated (approximately 300 K) before radical−radical, as well as ion−radical, reactions initiate.

When a radical pulse with a duration of 1.3 ms is merged and mixed with the continuous ion/He stream (flow velocity of the buffer gas is roughly 95 m s^{-1}), it generates a packet of radical/ion mixture in He (Figure 5), where the ion−radical reaction takes place as it flows toward the end of the reaction tube. Each packet is $[(1.3 \times 10^{-3}\ s) \times (9500\ cm/s)] \cong 12$ cm long and $[(12\ cm) \times (\pi \times (7.3/2)^2\ cm^2] \cong 500\ cm^3$ in volume.[38] As the ion−radical packet moves along the flow tube, axial diffusion of the radicals will expand the packet. However, we have estimated[35,39,40] that diffusion of the radicals is small and

can be ignored. We estimate that the density of the allyl radical or *o*-benzyne is roughly $(3 \times 10^{13}$ radicals$)/(500$ cm$^3) \cong 6 \times 10^{10}$ radicals cm^{-3} in each packet. With a pulsed valve repetition rate of 20 Hz, one packet is separated from the next one by 500 cm. Therefore, the duty cycle of the experiment is $(1.3 \times 10^{-3}$ s$) \times (20$ s$^{-1}) = 0.026$. An increase in the valve repetition rate would not change the kinetic analysis, since it increases the duty cycle[41] of the experiment without changing the radical density, and hence the reaction chemistry, in each packet. The radical density can be changed by varying the precursor concentration in the sample flask, which has been confirmed experimentally. The He flow carries the packets 1 m down the reaction flow tube to the detection quadrupole mass filter in 10 ms.

An estimate of signal intensities in ion−radical reactions can be made as follows. For the reaction of $H_3O^+ + CH_2CHCH_2 \rightarrow$ products, the density of the allyl radicals is $\rho(CH_2CHCH_2) \cong 6 \times 10^{10}$ radicals cm^{-3} after the radical/He gas pulse (1.3 ms duration) completely mixes with the ion/He flow. The ion loss within the reaction zone follows pseudo-first-order kinetics because the radical density is many orders of magnitude greater. Suppose a duty cycle of 1, so that the radical flow is continuous. Calling τ the ion/radical reaction time and $I_0(H_3O^+)$ the ion intensity at the downstream end of the flow tube in the absence of reactant neutrals, we assume the proton transfer to go at the collision rate. Consequently, the bimolecular ion/radical rate coefficient, k^{II}(ion, radical), is 1.5×10^{-9} cm^3 s^{-1} and the intensity of the H_3O^+ ions at the detection end $I(H_3O^+)$ is given by

$$I(H_3O^+) = I_0(H_3O^+) \exp[-k^{II}(\text{ion, radical})\, \rho(CH_2CHCH_2)\, \tau] \quad (12)$$

The reaction time equals the gas transit time of 10 ms divided by the factor of 1.6, because, on average, the ions travel 1.6 times faster than the buffer and neutral reactant gases due to the hydrodynamics of the flow system.[42] The equation is then solved for $(I/I_0) = \exp[-(1.5 \times 10^{-9})\, (6 \times 10^{10})\, (10 \times 10^{-3})/1.6] = 0.57$. This suggests that 43% of the H_3O^+ ions will be converted to products. For the actual duty cycle[41] of 0.026, the expected conversion of H_3O^+ to products is then 1.1%. Though direct measurements of H_3O^+ depletion are difficult, substantial amounts of product ions are expected to be observed. If the SIFT produces 10 000 H_3O^+ ions s^{-1}, then the H_3O^+ depletion $= \Sigma$(reaction products) $\cong 0.011 \times 10\,000$. Consequently, we anticipate about 110 counts s^{-1} of product ions, far exceeding the instrumental detection limits. The biggest uncertainty in this estimate is the density of the allyl radicals, $\rho(CH_2CHCH_2)$.

Results and Discussion

Allyl Radical + H_3O^+. Figure 6 illustrates the products from the reaction of H_3O^+ with allyl radicals produced at 1000 and 1100 K (eq 3). The bottom trace displays a reference spectrum resulting from the reaction of SIFTed H_3O^+ and allyl iodide at 300 K. At room temperature, the high mass ion is the protonated allyl iodide, $[CH_2{=}CH{-}CH_2I, H]^+$ *m*/*z* 169, arising from exothermic proton transfer: $C_3H_5I + H_3O^+ \rightarrow [C_3H_6I^+ \cdots H_2O] \rightarrow C_3H_6I^+ + H_2O$. The transient complex also undergoes intracomplex elimination of hydrogen iodide to form $C_3H_5^+(H_2O)$ *m*/*z* 59: $[C_3H_6I^+ \cdots H_2O] \rightarrow [C_3H_5^+ \cdots HI \cdots H_2O] \rightarrow C_3H_5^+(H_2O) + HI$. Subsequently, $C_3H_5^+(H_2O)$ loses H_2O to yield $C_3H_5^+$ *m*/*z* 41. The peak at *m*/*z* 37 is $H_3O^+(H_2O)$ due to clustering of the primary H_3O^+ ions with trace amounts of water in the flow tube. Consideration of the kinetics finds that the *m*/*z* 59 ion must derive directly from the transient complex; clustering of the isolated $CH_2CHCH_2^+$ product ion with trace water would produce a *m*/*z* 59 signal smaller by orders of magnitude.

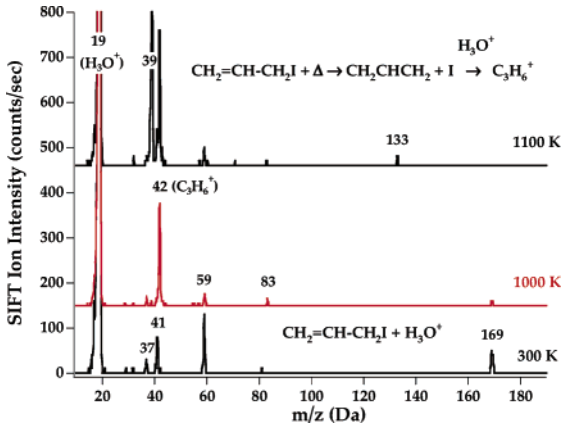

Figure 6. SIFT mass spectrum for the reaction of H_3O^+ with allyl radicals produced at 1000 and 1100 K (top 2 traces). The signal at *m*/*z* 42 ($C_3H_6^+$) results from protonation of the allyl radical, $CH_2CHCH_2 + H^+$. The bottom trace is a reference spectrum showing ions resulting from the reaction of H_3O^+ and the precursor, allyl iodide.

At 1000 K (which is known from Figure 3 to produce the allyl radical), the signal at *m*/*z* 42 ($C_3H_6^+$) is essentially the sole product observed (≅225 counts s^{-1}) resulting from protonation of the allyl radical (eq 3).[1] In addition, there are still traces of *m*/*z* 169 and 59 products due to the reaction of residual precursor molecules. A small peak at *m*/*z* 83 is assigned to protonated 1,5-hexadiene, $[CH_2{=}CH{-}CH_2CH_2CH{=}CH_2, H]^+$, where hexadiene is the product of allyl radical recombination. Indeed, if we use a higher precursor concentration we observe a substantial increase in the dimer ($C_6H_{11}^+$) signal relative to the monomer $C_3H_6^+$ signal (nearly half of the $C_3H_6^+$ signal, which also increased to more than 1000 counts s^{-1} at the elevated concentration). At 1100 K, the precursor allyl iodide is completely depleted, while unknown peaks are observed at *m*/*z* 39, 41, and 133 due to species that are emitted from the hot nozzle itself (see below).

The proton transfer reaction is 12 kcal mol^{-1} exothermic based on the proton affinities (*PA*s) of the allyl radical (177.4 ± 0.8 kcal mol^{-1}) and water[43] (165.1 ± 0.7 kcal mol^{-1}). The $PA(CH_2CHCH_2)$ has been derived from the heat of formation for propene,[44] $\Delta_f H_{298}(CH_3CHCH_2) = 4.8 \pm 0.2$ kcal mol^{-1} and the adiabatic[45] $IE(CH_3CHCH_2) = 9.73 \pm 0.01$ eV, giving $\Delta_f H_{298}(CH_3CHCH_2^+) = 229.2 \pm 0.3$ kcal mol^{-1}, which is then combined with the heat of formation for the allyl radical,[46] $\Delta_f H_{298}(CH_2CHCH_2) = 40.9 \pm 0.7$ kcal mol^{-1}. The product ion $C_3H_6^+$ is most likely [propene]$^+$, which is about 7 kcal mol^{-1} more stable than [cyclopropane]$^+$ ($\Delta_f H_{298} = 236.8$ kcal mol^{-1}).[27]

The observed $C_3H_6^+$ signal of 225 counts s^{-1} at 1000 K is in reasonable agreement with the above kinetic estimate. The somewhat greater signal may be due to a higher conversion efficiency of $CH_2{=}CH{-}CH_2I \rightarrow CH_2CHCH_2$ and/or higher detection sensitivity of $C_3H_6^+$. The agreement suggests that the proton transfer reaction occurs at nearly every collision ($k_3^{II} = 1.49 \times 10^{-9}$ cm^3 s^{-1}) and that radical density and ion reaction kinetics have been reasonably well characterized.

Allyl Radical + HO^-. When HO^- encounters allyl radicals generated from the nozzle at 1000 K, the deprotonated allyl radical, $C_3H_4^-$ *m*/*z* 40, was not observed within detection limits (Figure 7). Instead, a minor peak was observed at *m*/*z* 81; dimerization of allyl radicals to produce 1,5-hexadiene, followed by deprotonation, will lead to $CH_2{=}CH{-}CHCH_2{-}CH{=}CH_2^-$

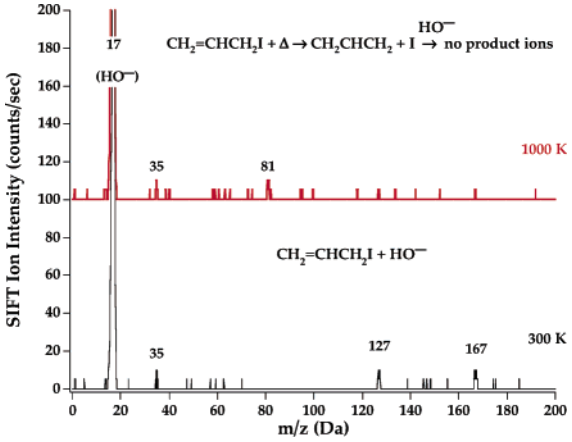

Figure 7. SIFT mass spectrum for the reaction of HO^- with allyl radicals produced at 1000 K (top trace). No trace of the deprotonated allyl radical, $C_3H_4^-$ *m/z* 40, is observed. The bottom trace is a reference spectrum showing ions resulting from reaction of HO^- and the precursor, allyl iodide.

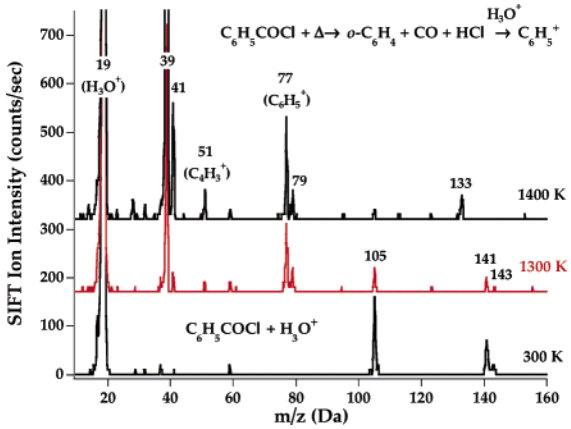

Figure 8. SIFT mass spectrum for the reaction of H_3O^+ with *o*-benzyne produced at 1300 and 1400 K (top 2 traces). The signal at *m/z* 77 ($C_6H_5^+$) results from protonation of *o*-benzyne, [*o*-C_6H_4, H^+]. The bottom trace is a reference spectrum showing ions resulting from the reaction of H_3O^+ and the precursor, benzoyl chloride.

m/z 81. In the 300 K spectrum, the *m/z* 167 peak is due to HO^- deprotonation of allyl iodide [$\Delta_{acid}H_{298}(H_2O) = 390.3$ kcal mol^{-1} and $\Delta_{acid}H_{298}$(allyl iodide) = 370.7 kcal mol^{-1}][27] to yield $CH_2{=}CH{-}CHI^-$. The *m/z* 127 peak arises from nucleophilic substitution (S_N2) reactions of HO^- at the allylic carbon of the precursor to produce I^- and $CH_2{=}CH{-}CH_2OH$. In both spectra, *m/z* 35 is $HO^-(H_2O)$ resulting from HO^- clustering with trace amounts of water in the flow tube.

If the reaction is assumed to proceed solely via proton abstraction and at the collision rate[47] ($k_{coll} = 1.54 \times 10^{-9}$ cm^3 s^{-1}), the estimated intensity[48] for the $C_3H_4^-$ (*m/z* 40) signal is 90 counts s^{-1} at 1000 K. The noise level observed at *m/z* 40 in Figure 7 corresponds to an upper limit of 2% efficiency for the deprotonation reaction. Although the $\Delta_{acid}H_{298}(CH_2CHCH_2)$ is unknown, we conclude that the reaction $CH_2CHCH_2 + HO^- \rightarrow C_3H_4^- + H_2O$ does not occur.

Since no product ions are observed, one might conclude that CH_2CHCH_2 and HO^- simply do not react. However, an alternative explanation is that the allyl radical and hydroxide ion are associatively or reactively detaching.

$$CH_2CHCH_2 + HO^- \rightarrow CH_2{=}CH{-}CH_2OH + e \quad (13a)$$

$$\rightarrow CH_2{=}C{=}CH_2 + H_2O + e \quad (13b)$$

Associative detachment to produce allyl alcohol (37 kcal mol^{-1} exothermic, eq 13a), or reactive detachment to yield allene and water (20 kcal mol^{-1} exothermic, eq 13b) is consistent with our observations. These processes are analogous to the reactions of negative ions with *atomic* radicals[2,19,49] and hence are expected to be very efficient.

Thermal dissociation of $CH_2{=}CHCH_2I$ will produce the same amounts of allyl radicals and iodine atoms. It is intriguing to ask why iodide anions are not observed despite the exothermicity of the charge transfer reaction[50] between I and HO^- [*EA*(I) = 3.059 eV and *EA*(HO) = 1.828 eV]. The collision rate[47] for I + HO^- is also calculated to be fairly large ($k_{col} = 1.31 \times 10^{-9}$ cm^3 s^{-1}). This could be explained by considering the state-specific charge transfer cross sections for $I + HO^-(v' = 0) \rightarrow I^- + HO(v)$. In analogous exothermic charge transfer[51] of $N_2^+(v') + Kr \rightarrow N_2(v) + Kr^+(^2P_J)$, the reaction is efficient only when (i) the reaction is near energy resonant such that the energy gap is small ($|\Delta E| < 100$ meV) and (ii) the associated Franck−Condon factor is large. From the very similar internuclear distances for HO (0.9697 Å)[52] and HO^- (0.9643 Å),[53] formation of $HO(v = 0)$ is expected to have a large Franck−Condon overlap, whereas it is too highly exothermic by 1.231 eV. On the other hand, reactions that form $HO(v = 2)$ and $HO(v = 3)$ are more energy resonant ($\Delta E = -367$ and $+33$ meV, respectively) but the Franck−Condon overlaps would be small. We compute the Franck−Condon factors for the $HO^-(v' = 0) \rightarrow HO(v)$ transitions using the spectroscopic constants[52,53] and the procedure of Nicholls.[54] The values we find are 0.9988 ($v = 0$), 1.09×10^{-3} ($v = 1$), 8.05×10^{-5} ($v = 2$), and 2.99×10^{-6} ($v = 3$), substantiating the absence of I^- product.

***o*-Benzyne + H_3O^+.** Figure 8 shows the reaction of H_3O^+ ions with *o*-benzyne produced at 1300 and 1400 K. The bottom trace is a reference spectrum resulting from reaction of SIFTed H_3O^+ and benzoyl chloride at 300 K. At room temperature, the high mass ion is the protonated benzoyl chloride, [C_6H_5COCl, $H]^+$ *m/z* 141, 143 at natural chlorine abundance: $C_6H_5COCl + H_3O^+ \rightarrow [C_6H_5COClH^+ \cdots H_2O] \rightarrow C_6H_5COClH^+ + H_2O$. Fragmentation of the parent ion affords the acyl cation, C_6H_5-CO^+ *m/z* 105, and HCl.

At 1300 K, which is known to produce *o*-benzyne, the major product is observed at *m/z* 77 ($C_6H_5^+$) which is derived from protonation of *o*-benzyne, *o*-$C_6H_4 + H^+$ (eq 5). There are still traces of the protonated precursor $C_6H_5COClH^+$ *m/z* 141, 143 and its fragmentation product $C_6H_5CO^+$ *m/z* 105. Thermal fragmentation of benzoyl chloride produces *o*-benzyne, a small amount of which further fragments: *o*-$C_6H_4 + \Delta \rightarrow HC{\equiv}CH$ and $HC{\equiv}C{-}C{\equiv}CH$. Acetylene[27] (*PA* = 153.3 kcal mol^{-1}) will not proton transfer with H_3O^+ but diacetylene[27] will (*PA* = 176.2 kcal mol^{-1}), giving the ion [$HC{\equiv}C{-}C{\equiv}CH$, H^+] at *m/z* 51. The ion at *m/z* 79 is likely protonated benzene, [C_6H_6, $H]^+$; there is PIMS and matrix IR evidence for production of benzene ($C_6H_6^+$ *m/z* 78) at high temperatures (Figures 3 and 4). One might consider *m/z* 77 and 79 to be a chlorinated species, C_3H_6-Cl^+, but the PIMS spectrum (Figure 3) and the matrix IR spectrum (Figure 4) do not indicate the presence of C_3H_5Cl radicals from the thermal dissociation of benzoyl chloride. The peaks at *m/z* 39 and 41 belong to unknown species arising from the hot nozzle itself. At 1400 K, the precursor benzoyl chloride is completely depleted, while unknown peaks are observed at *m/z* 39, 41, and 133. These peaks are still present when the pulsed valve is closed, confirming that they are due to species emitted from the hot SiC nozzle.

The $C_6H_5^+$ product is likely to be the phenyl cation resulting from addition of a proton to the triple bond of *o*-benzyne.

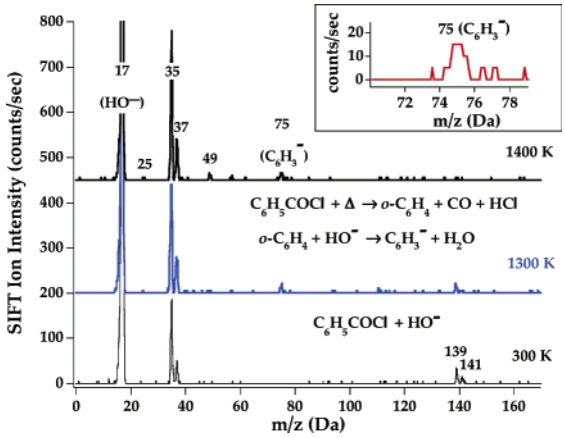

Figure 9. SIFT mass spectrum for the reaction of HO^- with *o*-benzyne produced at 1300 and 1400 K (top 2 traces). The signal at *m*/*z* 75 ($C_6H_3^-$) results from deprotonation of *o*-benzyne. The bottom trace is a reference spectrum showing ions resulting from the reaction of HO^- and the precursor, benzoyl chloride.

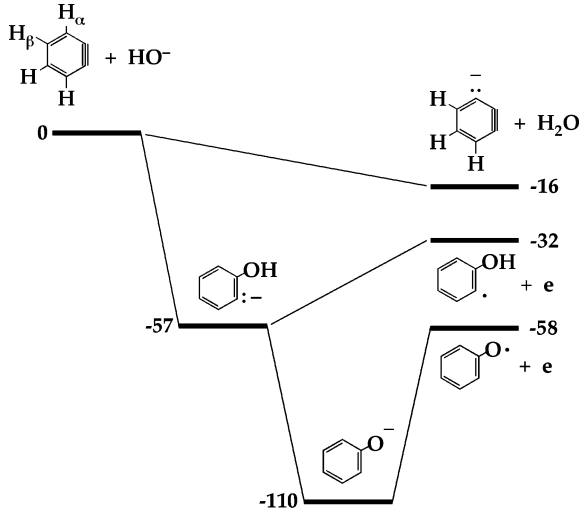

Figure 10. Energetics for the reaction of HO^- with *o*-benzyne to form ionic or associative detachment products.

However, the assignment awaits direct measurement of the proton affinity for *o*-benzyne. The reported[43,55] $PA(o\text{-}C_6H_4)$ of 201 kcal mol^{-1} is derived from an ion cycle including the heats of formation for *o*-C_6H_4 and $C_6H_5^+$, where $\Delta_f H_{298}(C_6H_5^+)$ is apparently determined[55] from the heat of formation[56,57] and the adiabatic $IE(C_6H_5)$[58] for the phenyl radical. The SIFT hyperthermal nozzle apparatus is capable of generating *o*-benzyne diradicals and their protonated species, which allows for direct study of the *o*-benzyne proton affinity to examine this hypothesis. Reactivity and CID studies of the $C_6H_5^+$ species would also be enlightening.

The observed $C_6H_5^+$ signal is approximately 140 counts s^{-1} at 1300 K. This is in fair agreement with the 160 counts s^{-1} estimated with the assumption of an encounter controlled proton transfer rate[47] ($k_{col} = 2.59 \times 10^{-9}$ cm^3 s^{-1}). The small deficit is likely due to loss of the benzoyl chloride precursor by adsorption in the transfer line; frequent passivation of the inlet system was necessary to maintain the stable $C_6H_5^+$ signal. The lower conversion and higher fragmentation upon pyrolysis, and mass discrimination against *m*/*z* 77 in the detection mass filter, may also contribute to the reduced signal. It is thus reasonably concluded that exothermic proton transfer of *o*-benzyne with H_3O^+ proceeds at nearly every collision.

***o*-Benzyne + HO^-.** Figure 9 displays the SIFT mass spectra for the reaction of HO^- with *o*-benzyne produced at 1300 and 1400 K. The bottom trace is the reference spectrum resulting from reaction of SIFTed HO^- and the precursor, benzoyl chloride, at 300 K. At room temperature, the high mass ion is the deprotonated benzoyl chloride, $C_6H_4COCl^-$ *m*/*z* 139, 141 at natural chlorine abundance: $C_6H_5COCl + HO^- \rightarrow C_6H_4COCl^- + H_2O$. The large signal[59] of Cl^- (*m*/*z* 35, 37) results from nucleophilic substitution by HO^-: $C_6H_5COCl + HO^- \rightarrow [C_6H_5C(O)OH \cdots Cl^-] \rightarrow C_6H_5COOH + Cl^-$. Chloride ions are derived directly from the complex since HCl ($\Delta_{acid}H_{298}$ = 333.4 kcal mol^{-1}) is more acidic than benzoic acid (340.1 kcal mol^{-1}).[27]

At 1300 and 1400 K, the most important new signal is observed at *m*/*z* 75 ($C_6H_3^-$, ≅15 counts s^{-1}), which is assigned to the product from deprotonation of *o*-benzyne, [*o*-C_6H_4 - H^+] (eq 6). Benzoyl chloride is nearly depleted at 1400 K. Chloride ions at *m*/*z* 35 and 37 must be derived from the deprotonation reaction of HO^- (eq 6) with a pyrolysis product HCl. Peaks at *m*/*z* 25 and 49 are deprotonated acetylene, $HC{\equiv}C^-$, and diacetylene, $HC{\equiv}C{-}C{\equiv}C^-$, respectively. Acetylene[27] ($\Delta_{acid}H_{298}$ = 379.0 kcal mol^{-1}) and diacetylene[27] (360.3 kcal mol^{-1}) are thermal cracking products of *o*-C_6H_4.

Figure 10 shows the possibilities for reaction of HO^- with *o*-C_6H_4. A hydroxide ion can deprotonate benzyne to generate the $C_6H_3^-$ anion, or it can add to the hydrocarbon ring forming the activated complex, $C_6H_4OH^-$.

Deprotonation of *o*-benzyne is exothermic since the gas phase basicity[27] of hydroxide ($\Delta_{acid}G_{298}$ = 383.7 ± 0.3 kcal mol^{-1}) exceeds the reported acidity of *o*-benzyne[27,60] (372 ± 5 kcal mol^{-1}) by more than 10 kcal mol^{-1}. More recent experiments and extensive calculations suggest that the reported value for the gas phase acidity is an overestimation; a better estimate for $\Delta_{acid}G_{298}$(*o*-C_6H_4) is about 366 kcal mol^{-1} ($\Delta_{acid}H_{298} \cong$ 374 kcal mol^{-1}).[61] Abstraction of a proton α to the triple bond must occur; the *β* proton is predicted[61] by electronic structure calculations (MP4(SDQ)/6-31+G*//MP2/6-31+G*) to be significantly less acidic by about 13 kcal mol^{-1}. We estimate that the proton abstraction channel to form the α-$C_6H_3^-$ is exothermic by 16 kcal mol^{-1}; see Figure 10.

The $C_6H_3^-$ signal at 1400 K is only 15 counts s^{-1} as compared to 115 counts s^{-1} expected from a collisional reaction rate[47] ($k_{col} = 2.71 \times 10^{-9}$ cm^3 s^{-1}) and a scaling factor.[62] The low intensity of the $C_6H_3^-$ signal is also evident from the large signals observed for Cl^- ions (*m*/*z* 35, 37). Stoichiometrically, the same amounts of *o*-benzyne and hydrogen chloride are formed from pyrolysis of the precursor, and the collision rate for HO^- + *o*-C_6H_4 is even greater than the rate[47] for HO^- + HCl ($k_{col} = 1.96 \times 10^{-9}$ cm^3 s^{-1}). This suggests that the *o*-benzyne deprotonation is slower than the collision rate by nearly an order of magnitude ($k_6^{II} \cong 10^{-10}$ cm^3 s^{-1}).

A slow deprotonation is an unexpected result because exothermic proton abstraction is usually a barrierless process that takes place at every collision.[2] The only exception to this rule is thermoneutral, identity proton transfer between carbon acids and their conjugate bases, for which the transition state energies can be similar to or higher than the energies of the reactant pairs.[63,64] It might be possible that the proton abstraction is rendered inefficient by the existence of a double well potential[65,66] or a dynamic barrier.[67] These effects are known to be minor.

Instead of reacting by proton abstraction, eq 6, the HO^- ion might rapidly add to *o*-benzyne and form a highly activated

complex, $(C_6H_4OH^-)^*$. Such an adduct is likely to autodetach: $(C_6H_4OH^-)^* \rightarrow C_6H_4OH + e$. Consequently, no negative ions would be formed and only thermal electrons would be observed. Associative detachment might explain the low signal levels observed for $C_6H_3^-$.

Consider the energetics of associative detachment (Figure 10). Addition of the HO^- ion to the triple bond to form the *o*-hydroxyphenyl anion is very exothermic (57 kcal mol^{-1}). The heat of formation[55,68,69] and singlet−triplet splitting[70] for *o*-benzyne are 105 kcal mol^{-1} and 37.5 ± 0.3 kcal mol^{-1}, respectively. A hydroxyl radical adds to the triplet *o*-benzyne to form the *o*-hyroxyphenyl radical (o-$C_6H_4OH^\bullet$). The heat of addition is taken as the C_6H_5-OH bond dissociation energy for phenol [$DH_{298}(C_6H_5-OH) = 112$ kcal mol^{-1}][46] leading to $\Delta_f H_{298}(o\text{-}C_6H_4OH^\bullet) \cong 40$ kcal mol^{-1}. Approximating $EA(o\text{-}C_6H_4OH^\bullet)$ as $EA(C_6H_5) = 25.3 \pm 0.1$ kcal mol^{-1} (1.096 ± 0.006 eV)[71], we estimate the heat of formation for the *o*-hydroxyphenyl anion to be about 15 kcal mol^{-1} and thus $\Delta_{rxn}H_{298}(o\text{-}C_6H_4 + HO^- \rightarrow o\text{-}C_6H_4OH^-) \cong -57$ kcal mol^{-1} (2.5 eV). If the binding energy of the electron is 1.1 eV, the reaction exothermicity generates an activated ion, $[o\text{-}C_6H_4OH^-]^*$, with energy (2.5 eV) far in excess of $EA(o\text{-}C_6H_4OH^\bullet)$. Rapid electron detachment is expected to ensue. If the *o*-hydroxy phenyl anion further isomerizes to form a phenoxide ion ($\Delta_f H_{298} = -38.3$ kcal mol^{-1}),[27] the reaction exothermicity (110 kcal mol^{-1}, ≅4.8 eV) exceeds the electron binding energy (2.253 ± 0.006 eV)[71] even more significantly (Figure 10).

Trapping and detection of thermal electrons in the flow tube with electron scavengers such as SF_6 could confirm the assignments for the detachment reactions of HO^- ions with the allyl radical and *o*-benzyne diradical. If associative detachment of hydroxide by *o*-benzyne can be demonstrated, it would be a novel reaction channel for HO^- ions[2] that is facilitated by the high energy content in the reactant *o*-benzyne. Alkynes, such as acetylene, are simply deprotonated by hydroxide: $HC{\equiv}CH + HO^- \rightarrow HC{\equiv}C^- + H_2O$.

Conclusion

These initial investigations have demonstrated that a flowing afterglow/SIFT device with a supersonic, hyperthermal nozzle can be used for experimental investigations of ions with polyatomic organic radicals and diradicals. A practical consequence of this development is that one can undertake laboratory studies of the ion chemistry that produces a large number of interstellar organic radicals and diradicals. The observation that negative ions reacting with organic radicals may have competing proton transfer vs associative detachment channels is an unexpected fundamental result.

Acknowledgment. S.K. and V.M.B. gratefully acknowledge support of the National Science Foundation (CHE-0349937); X.Z. and G.B.E. are supported by a grant from the Chemical Physics Program, United States Department of Energy (DE-FG02-87ER13695) and the NSF (CHE-9813659). We thank Carleton Howard and Evan B. Jochnowitz for very helpful discussions. Don David and CIRES Instrument Shop are thanked for their continued excellent work and support.

References and Notes

(1) Zhang, X.; Bierbaum, V. M.; Ellison, G. B.; Kato, S. *J. Chem. Phys.* **2004**, *120*, 3531.

(2) Ikezoe, Y.; Matsuoka, S.; Takebe, M.; Viggiano, A. *Gas Phase Ion−Molecule Reaction Rate Constants Through 1986*; Maruzen: Tokyo, 1987.

(3) Bowers, M. T. *Gas Phase Ion Chemistry*; Academic Press: New York, 1979; Vol. I.

(4) Bowers, M. T. *Gas Phase Ion Chemistry*; Academic Press: New York, 1979; Vol. II.

(5) Bowers, M. T. *Gas Phase Ion Chemistry*; Academic Press: New York, 1984; Vol. III.

(6) *The Encyclopedia of Mass Spectrometry*; Gross, M. L., Caprioli, R., Eds.; Elsevier: Amsterdam, 2003; Vol. 1.

(7) Villalta, P. W.; Huey, L. G.; Howard, C. J. *J. Phys. Chem.* **1995**, *99*, 12829.

(8) Scholtens, K. W.; Messer, B. M.; Cappa, C. D.; Elrod, M. J. *J. Phys. Chem. A* **1999**, *103*, 4378.

(9) Hanson, D. R.; Orlando, J. J.; Nozière, B.; Kosciuch, E. *Int. J. Mass Spectrom.* (submitted).

(10) Born, M.; Ingemann, S.; Nibbering, N. M. M. *Mass Spectrom. Rev.* **1997**, *16*, 181.

(11) Kenttämaa, H. I. Distonic Radical Cations. In *The Encyclopedia of Mass Spectroscopy*; Armentrout, P. B., Ed.; Elsevier: Amsterdam, 2003; Vol. 1, p 619.

(12) Hayhurst, A. N.; Kittelson, D. B. *Combust. Flame* **1978**, *31*, 37.

(13) *The Diffuse Interstellar Bands*; Tielens, A. G. G. M., Snow, T. P., Eds.; Kluwer Academic: Dordrecht, 1995.

(14) Salama, F.; Galazutdinov, G. A.; Krelowski, J.; Allamandola, L. J.; Musaev, F. A. *Astrophys. J.* **1999**, *526*, 265.

(15) Sloan, G. C.; Hayward, T. L.; Allamandola, L. J.; Bregman, J. D.; DeVito, B.; Hudgins, D. M. *Astrophys. J.* **1999**, *513*, L65.

(16) McCarthy, M. C.; Thaddeus, P. *Chem. Soc. Rev.* **2001**, *30*, 177.

(17) Le Page, V.; Lee, H. S.; Bierbaum, V. M.; Snow, T. P. *NASA Conference Publication* **1996**, *3343*, 125.

(18) Demirev, P. A. *Rapid Commun. Mass Spectrom.* **2000**, *14*, 777.

(19) Barckholtz, C.; Snow, T. P.; Bierbaum, V. M. *Astrophys. J.* **2001**, *547*, L171.

(20) Blush, J. A.; Clauberg, H.; Kohn, D. W.; Minsek, D. W.; Zhang, X.; Chen, P. *Acc. Chem. Res.* **1992**, *25*, 385.

(21) Van Doren, J. M.; Barlow, S. E.; DePuy, C. H.; Bierbaum, V. M. *Int. J. Mass Spectrom. Ion Processes* **1987**, *81*, 85.

(22) Zhang, X.; Friderichsen, A. V.; Nandi, S.; Ellison, G. B.; David, D. E.; McKinnon, J. T.; Lindeman, T. G.; Dayton, D. C.; Nimlos, M. R. *Rev. Sci. Instrum.* **2003**, *74*, 3077.

(23) Kato, S.; Frost, M. J.; Bierbaum, V. M.; Leone, S. R. *Rev. Sci. Instrum.* **1993**, *64*, 2808.

(24) Gilbert, T.; Fischer, I.; Chen, P. *J. Chem. Phys.* **2000**, *113*, 561.

(25) A more recent measurement reports 8.133 ± 0.001 eV and the small discrepancy remains unresolved. [Liang, C.; Chen, C.; Wei, C.; Chen, Y. *J. Chem. Phys*. **2002**, *116*, 4162].

(26) Zhang, X.; Chen, P. *J. Am. Chem. Soc.* **1992**, *114*, 3147.

(27) Unless otherwise specified, all thermochemical values have been taken or derived from *NIST Chemistry Webbook*, NIST Standard Reference Database Number 69; March, 2003 release and references therein.

(28) Radziszewski, J. G.; Hess, B. A., Jr.; Zahradnik, R. *J. Am. Chem. Soc.* **1992**, *114*, 52.

(29) Jona, P.; Gussoni, M.; Zerbi, G. *J. Phys. Chem.* **1981**, *85*, 2210. The vibrational frequencies for HCC−CCH come from the *NIST Chemistry Webbook*.

(30) Stepanian, S. G.; Reva, I. D.; Radchenko, E. D.; Sheina, G. G. *Vib. Spectrosc.* **1996**, *11*, 123.

(31) Andrews, L.; Johnson, G. L.; Davis, S. R. *J. Phys. Chem.* **1985**, *89*, 1706.

(32) Friderichsen, A. V.; Radziszewski, J. G.; Nimlos, M. R.; Winter, P. R.; Dayton, D. C.; David, D. E.; Ellison, G. B. *J. Am. Chem. Soc.* **2001**, *123*, 1977.

(33) Nandi, S.; Arnold, P. A.; Carpenter, B. K.; Nimlos, M. R.; Dayton, D. C.; Ellison, G. B. *J. Phys. Chem. A* **2001**, *105*, 7514.

(34) Near the beginning of the SIFT reaction flow tube (20−30 cm), the ion/He flow is turbulent. Further downstream, the ion/He flow becomes laminar. Injecting the radical/He pulse into the turbulent region causes the mixing of the radicals and the ions to be relatively fast.

(35) Bierbaum, V. M. In *The Encyclopedia of Mass Spectrometry*; Armentrout, P. B., Ed.; Elsevier: Amsterdam, 2003; Vol. 1, p 98.

(36) Miller, D. R. In *Atomic and Molecular Beam Methods*; Scoles, G., Ed.; Oxford University: New York, 1988; Vol. 1.

(37) Liepmann, H. W.; Roshko, A. *Elements of Gasdynamics*; Wiley: New York, 1957.

(38) In fact, the packet (or ion/radical reaction zone) is not plug shaped, since the initial section of the reaction flow tube is characterized by turbulent flow. Downstream, the packet shape will be affected by the parabolic velocity profile of the laminar He flow. The exact shape and volume of the packet is difficult to calculate.

(39) We use Fick's 2nd law of diffusion to calculate the diffusion distance for the radicals in the packet (see F. M. White, *Heat and Mass Transfer*; Chapter 11 and Appendices L and M). After the 10 ms transit time, the packet has expanded by about 3 cm in length. The loss of inert radicals (such as allyl) at the wall following radial diffusion will be small.

(40) White, F. M. *Heat and Mass Transfer*; Addison-Wesley: New York City, 1988.

(41) Increasing the duty cycle will increase the product ion signal intensity. An increased duty cycle requires an increase in the repetition rate of the pulsed valve for the nozzle. However, since at high nozzle temperatures the pulse width becomes unstable when the frequency of the pulsed valve is high, we used the repetition rate of 20−40 Hz in our experiment to have a stable pulse width. Improving the stability of the pulse width at high frequency is in progress.

(42) Upschulte, B. L.; Shul, R. J.; Passarella, R.; Keesee, R. G.; Castleman, A. W., Jr. *Int. J. Mass Spectrom. Ion Processes* **1987**, *75*, 27. The initial section of the flow tube (20−30 cm in length) is actually turbulent flow. However, the total reaction time will not be significantly affected by this short section.

(43) Hunter, E. P. L.; Lias, S. G. *J. Phys. Chem. Ref. Data* **1998**, *27*, 413.

(44) Pedley, J. B.; Naylor, R. D.; Kirby, S. P. *Thermochemical Data of Organic Compounds*, 2nd ed.; Chapman and Hall: New York, 1986.

(45) Traeger, J. C. *Int. J. Mass Spectrom. Ion Processes* **1984**, *58*, 259.

(46) Blanksby, S. J.; Ellison, G. B. *Acc. Chem. Res.* **2003**, *36*, 255.

(47) We have calculated the ion−radical collision rate coefficients using the parametrized trajectory collision theory described by Su and Chesnavich [*J. Chem. Phys.* **1982**, *76*, 5183]. Polarizabilities and permanent dipole moments have been derived as 5.1×10^{-24} cm^3 and 0.07 D (allyl radical) and 8.6×10^{-24} cm^3 and 1.5 D (*o*-benzyne), respectively, from DFT electronic structure calculations at B3LYP/6-311G(d,p). For other species, polarizabilities and dipole moments have been taken from the *CRC Handbook of Chemistry and Physics*, 75th edition; Lide, D. R., Ed.

(48) Doing a calculation similar to that for $C_3H_5 + H_3O^+ \rightarrow C_3H_6^+$: from eq 12 and considering the duty cycle of 0.026, the expected conversion of HO^- to products is about 1.1%. The SIFT produces 4000 HO^- ions s^{-1}, so the calculated product ion $C_3H_4^-$ intensity is about 45 counts s^{-1}. Taking into account that for $C_3H_5 + H_3O^+ \rightarrow C_3H_6^+$ at a nozzle temperature of 1000 K, the observed $C_3H_6^+$ ion intensity (225) is two times that of the calculated intensity (110). Alternatively this can be called the scaling factor (= 225/110), which corrects for uncertainties common to the HO^- and H_3O^+ experiments with the allyl radical. Therefore, we can estimate that under the same conditions the observed $C_3H_4^-$ ion intensity should be about $45 \times 2 = 90$ counts s^{-1} for $C_3H_5 + HO^- \rightarrow C_3H_4^-$.

(49) Fehsenfeld, F. C. Associative Detachment. In *Interactions Between Ions and Molecules*; Ausloos, P., Ed.; Plenum: New York, 1975; p 387.

(50) Rienstra-Kiracofe, J. C.; Tschumper, G. S.; Schaefer, H. F., III; Nandi, S.; Ellison, G. B. *Chem. Rev.* **2002**, *102*, 231.

(51) Kato, S.; de Gouw, J. A.; Lin, C. D.; Bierbaum, V. M.; Leone, S. R. *J. Chem. Phys.* **1996**, *105*, 5455. See Lipeles, M. *J. Chem. Phys.* **1969**, *51*, 1252.

(52) Huber, K. P.; Herzberg, G. *Molecular Spectra and Molecular Structure. IV. Constants of Diatomic Molecules*; Van Nostrand Reinhold: New York, 1979.

(53) Rosenbaum, N. H.; Owrutsky, J. C.; Tack, L. M.; Saykally, R. J. *J. Chem. Phys.* **1986**, *84*, 5308.

(54) Nicholls, R. W. *J. Res. Natl. Bur. Stand. A* **1961**, *65A*, 451.

(55) Guo, Y.; Grabowski, J. J. *J. Am. Chem. Soc.* **1991**, *113*, 5923.

(56) Robaugh, D.; Tsang, W. *J. Phys. Chem.* **1986**, *90*, 5363.

(57) Tsang, W. Heats of Formation of Organic Free Radicals by Kinetic Methods. In *Energetics of Organic Free Radicals*; Simoes, J. A. M., Greenberg, A., Liebman, J. F., Eds.; Blackie Academic: London, 1996; p 22.

(58) Sergeev, Y. L.; Akopyan, M. E.; Vilesov, F. I. *Opt. Spektrosk.* **1972**, *32*, 230.

(59) A small amount of Cl^- comes from deprotonation of HCl by HO^-: $HCl + HO^- \rightarrow Cl^- + H_2O$, since HCl is more acidic than H_2O. The small amount of the impurity of HCl in benzoyl chloride is generated by hydrolysis of C_6H_5COCl: $C_6H_5COCl + H_2O \rightarrow C_6H_5COOH + HCl$.

(60) Gronert, S.; DePuy, C. H. *J. Am. Chem. Soc.* **1989**, *111*, 9253.

(61) Kato, S. et al., in preparation.

(62) Taking into account that for $C_6H_4 + H_3O^+ \rightarrow C_6H_5^+$ at a nozzle temperature of 1300 K, the observed $C_6H_5^+$ ion intensity (140) is smaller than the calculated intensity (160). The scaling factor (= 140/160) will correct for uncertainties common to the HO^- and H_3O^+ experiments with the *o*-C_6H_4. Therefore, we can estimate that under the same conditions the observed $C_6H_3^-$ ion intensity should be around 115 counts s^{-1} for $C_6H_4 + HO^- \rightarrow C_6H_3^-$.

(63) Bernasconi, C. F.; Wenzel, P. J.; Keeffe, J. R.; Gronert, S. *J. Am. Chem. Soc.* **1997**, *119*, 4008.

(64) Keeffe, J. R.; Gronert, S.; Colvin, M. E.; Tran, N. L. *J. Am. Chem. Soc.* **2003**, *125*, 11730.

(65) Dodd, J. A.; Baer, S.; Moylan, C. R.; Brauman, J. I. *J. Am. Chem. Soc.* **1991**, *113*, 5942.

(66) Kato, S.; Dang, T. T.; Barlow, S. E.; DePuy, C. H.; Bierbaum, V. M. *Int. J. Mass Spectrom.* **2000**, *195/196*, 625.

(67) Lim, K. F.; Brauman, J. I. *J. Chem. Phys.* **1991**, *94*, 7164.

(68) Riveros, J. M.; Ingemann, S.; Nibbering, N. M. M. *J. Am. Chem. Soc.* **1991**, *113*, 1053.

(69) Wenthold, P. G.; Paulino, J. A.; Squires, R. R. *J. Am. Chem. Soc.* **1991**, *113*, 7414.

(70) Wenthold, P. G.; Squires, R. R.; Lineberger, W. C. *J. Am. Chem. Soc.* **1998**, *120*, 5279.

(71) Gunion, R. F.; Gilles, M. K.; Polak, M. L.; Lineberger, W. C. *Int. J. Mass Spectrom. Ion Processes* **1992**, *117*, 601.